Midkine inhibits dormancy of disseminated melanoma cells.

Carolina Rodriguez-Tirado[1,2,3,4,5#], Thoufiqul Alam Riaz[1,2,3,4,5#], Alcina A. Rodrigues[6], Nupura Kale[7], Smrithi Jayashree Satheeshkumar[1,2,3,4,5], Ayax Perez-Gallegos[1,2,3,4,5], David Olmeda[8&], Maria S. Soengas[8], and Maria Soledad Sosa[1,2,3,4,5].

[1]Department of Microbiology and Immunology, Albert Einstein College of Medicine, Bronx, NY 10461, USA
[2]Department of Oncology, Albert Einstein College of Medicine, Bronx, NY 10461, USA
[3]Marilyn and Stanley M. Katz Institute for Immunotherapy for Cancer and Inflammatory Disorders, Albert Einstein College of Medicine, Bronx, NY 10461, USA
[4]Cancer Dormancy Institute, Albert Einstein College of Medicine, Bronx, NY 10461, USA
[5]Ruth L. and David S. Gottesman Institute for Stem Cell Research and Regenerative Medicine, Albert Einstein College of Medicine, Bronx, NY 10461, USA
[6]Rutgers University, Newark, NJ 07103, USA
[7]Helen Diller Comprehensive Family Cancer Center, University of San Francisco, CA 94158, USA
[8]Melanoma Laboratory, Molecular Oncology Programme, Spanish National Cancer Research Centre (CNIO), Madrid 28049, Spain
[&] Current address: Drivers and Biomarkers of Metastasis Laboratory, Cancer Biology Department, Instituto de Investigaciones Biomédicas Sols-Morreale. (IIBM) CSIC-UAM, Madrid, Spain.

Running Title: Midkine inhibits dormancy.

# equal contributions.

Correspondence: Maria Soledad Sosa, Department of Microbiology and Immunology, Albert Einstein College of Medicine, Bronx, NY 10461, USA. Phone: (+1) 718.430.2115. E-mail: maria.sosa@einsteinmed.edu

The authors declare no potential conflicts of interest.

ABSTRACT

A significant factor in cancer-related mortality in melanoma is the appearance of intrinsically aggressive distal metastases. This recurrence frequently results from the awakening of dormant disseminated cancer cells (DCCs). One of the most puzzling clinical features in this disease is that DCCs rapidly develop into metastases in certain melanoma patients, while remaining inactive in others. We have previously identified NR2F1 as a driver of dormancy, but the mechanisms underlying its regulation, particularly when DCC are “awakened”, are poorly understood. This study reveals that the growth factor Midkine (MDK) triggers a potent autocrine mechanism that deactivates NR2F1-dependent dormancy in DCC, ultimately favouring metastatic outgrowth. The effect of MDK was found linked to deregulation of the p-p38/p-ERK ratio in DCCs, in a process that was partly ALK-dependent. Supporting the physiological relevance of these data, MDK and NR2F1 were inversely correlated in DCCs in human lymph nodes (LN). In this regard, we observed that human LN biopsies negative for metastasis carried higher percentages of the dormant MDK^{LOW}/$NR2F1^{HIGH}$ DCC phenotype, an effect that was inverted in metastasis-positive LN. Moreover, activation of NR2F1 with a specific agonist decreased the metastasis-initiating capacity of MDK^{HIGH} DCCs by blocking MDK-driven mTORC1 activity. Dual therapy targeting MDK (via inhibition) and NR2F1 (via activation) markedly improved survival in mouse models of melanoma. This investigation reveals that MDK^{HIGH} melanomas share a mechanism that that disrupts the natural capacity of DCCs to enter dormancy. Moreover, this study suggests that combining an NR2F1 agonist with an MDK inhibitor could be a potential therapeutic strategy to prolong the dormancy phase of melanoma DCCs, thereby preventing metastasis formation.

INTRODUCTION

Disseminated cancer cells (DCCs) have long-been pursued as the source of metastatic relapses after the removal of primary tumors. A main feature of DCCs is that they can remain in a non-proliferative/quiescent state defined as dormancy until they reactivate and give rise to metastasis. Melanoma patients with detectable DCCs had an increased risk of dying of melanoma than patients without DCC detection[1,2]. In cutaneous melanoma, the timing for relapse could range from months to years[3], yet the mechanisms that control dormancy and reactivation of melanoma DCCs are unclear. Here we report a complex interplay between factors promoting metastasis and those maintaining dormancy in melanoma DCCs. These findings will advance our knowledge of the biology of DCCs and help optimizing therapies for melanoma patients.

Recent publications on metastatic melanoma showed that the depletion of the secreted heparin-binding factor Midkine (MDK) reduced lymph node and lung metastases in mouse melanoma models. In addition, high levels of MDK correlated with a poor prognosis[4,5]. The described mechanisms of action for the pro-metastatic capacity of MDK to form LN metastasis involved a paracrine signal from melanoma cells on lymphatic endothelial cells facilitating adhesion and transmigration between endothelial cells. Nevertheless, whether MDK could affect the metastatic outgrowth of already disseminated melanoma cells in the lung in an autocrine manner remains unknown. The nuclear receptor NR2F1 is responsible for the dormancy phase of DCCs in head and neck and breast cancer[6-8]. Moreover, NR2F1 expression in dormant DCCs from BM aspirates from breast and prostate cancer patients is associated with their long-term dormancy[9,10]. Whether an autocrine MDK regulates NR2F1 has not been shown.

Here, we report that depletion of MDK in SK-Mel-147 melanoma cells (carrying high MDK levels and BRAF WT) reduced lung metastatic burden by increasing the percentage of dormant DCCs with high levels of NR2F1 expression. MDK suppresses NR2F1 expression via an autocrine mechanism involving ALK receptor signaling and inhibition of p38 MAPK activity, thereby downregulating NR2F1 targets such as SOX9, p27, and RARβ. Pre-clinical results showed that the use of an NR2F1 agonist reduced the size of lung metastatic foci formed by SK-Mel-147 MDK^{HIGH} cells by increasing the percentages of DCCs positive for NR2F1 and by inhibiting mTOR signaling. Combining the NR2F1 agonist with MDK depletion further diminished lung metastasis size in mice injected with MDK^{HIGH} melanoma cells, regardless of BRAF mutation status (WT or V600E). This combination therapy also significantly improved survival outcomes. These findings highlight the therapeutic potential of dormancy-inducing strategies, such as NR2F1 activation alone or paired with MDK targeting, to extend the dormant phase of MDK-high melanoma DCCs and curb metastatic progression.

RESULTS

MDK depletion induces NR2F1 expression in melanoma lung DCCs while preventing metastasis formation.

We have previously reported that, in melanoma patients, high levels of the growth factor MDK was associated with worse overall and disease-free survival[4,5]. Mice subcutaneously (s.c.) injected with melanoma cells with high levels of MDK (MDK^{HIGH}) formed lung metastases whereas mice injected with MDK^{LOW} melanoma cell lines did not[5]. Moreover, downregulation of MDK in MDK^{HIGH} melanoma cells showed reduced spontaneous lung metastases. We and others have previously shown that the nuclear receptor NR2F1 is responsible for the dormancy phase of head and neck squamous carcinoma cells[6]. Further, high NR2F1 levels in minimal residual disease stage have been linked to better survival in prostate and breast cancer patients[6,9,10]. Thus, we hypothesized that MDK^{LOW} melanoma cell lines, for example WM164 cells, which do not form lung metastasis[5], should have high levels of NR2F1 to account for the lack of metastasis capacity once disseminated to distant organs. To this end, we measured the levels of NR2F1 in lung disseminated cancer cells (DCCs) of mice s.c. injected with MDK^{HIGH} (SK-Mel-147, SK-Mel-28, and 451LU) and MDK^{LOW} (WM35 and WM164) melanoma cell lines. Of note, SK-Mel-147 cells expressed the highest protein levels of MDK when compared with the other five cell lines[5]. We observed that DCCs from the MDK^{high} melanoma cells SK-Mel-147 had ~20% DCCs positive for NR2F1% (**Fig. 1A&B)** and SK-Mel-28, and 451LU cells (**Supp. Fig. 1A**) had ~45%. By contrast, DCCs from the MDK^{low} melanoma cell lines WM164 (**Fig. 1A)** and WM35 (**Supp. Fig. 1A**) were ~65% positive for NR2F1. Interestingly, the MDK^{low} WM35 cell line, like the WM164 cells, is poorly metastatic when compared to MDK^{HIGH} cell lines[5]. Therefore, high MDK levels correlate with higher metastatic potential and with lower NR2F1 levels in DCCs.

We previously showed that nude mice s.c. injected with GFP-SK-Mel-147 cells carrying shRNA against MDK (shMDK) showed fewer lung metastasis[5]. Close inspection of the lungs of mice s.c. injected with GFP-SK-Mel-147 shMDK cells showed the presence of single DCCs detected with antibodies against GFP and anti-human vimentin antibody, which only recognizes the human protein (**Fig. 1B, Suppl. Fig. 1A-C**). Moreover, the total burden of lung DCCs did not change between SK-Mel-147 shControl- and shMDK groups (**Suppl. Fig. 1D**), showing that the capacity to disseminate to the lungs was not altered upon MDK depletion.

To confirm that MDK directly affected metastatic outgrowth of SK-Mel-147 cells without selective pressures from the primary tumors, we performed experimental metastasis assays. We observed less metastatic load in mice injected with GFP-SK-Mel-147 shMDK cells when compared to shControl cells, 28 days after intravenous injection (**Fig. 1C**). This suggests that, during the extension of the experiment, loss of MDK blunted their capacity to proliferate and form metastasis. Interestingly, we observed an increased percentage of NR2F1 positive DCCs in mice s.c. (~50% average) or i.v. (~60% average) injected with SK-Mel-147 shMDK cells when compared to

the SK-Mel-147 shControl- group (~25% average) (**Fig. 1B&C, Suppl. Fig. 1B**). Thus, these results show that the loss of MDK prevents lung metastasis formation and suggest a mechanism dependent on the induction of NR2F1 in DCCs. As predicted, NR2F1 levels (mRNA and protein) were increased upon MDK depletion in cultured melanoma cells (**Suppl. Fig. 1E &F**). Interestingly, growing lung metastases from spontaneous and experimental metastasis assays were negative for NR2F1 (**Suppl. Fig. 1B&C**), which is consistent with previous studies and confirms the association of NR2F1 expression with cell cycle arrest[6-8]. Importantly, the NR2F1 levels in non-metastatic WM164 cells with low levels of MDK expression[5] compared to metastatic MDK^{HIGH} SK-Mel-147 cells were downregulated upon addition of recombinant human MDK (rhMDK) (**Supp. Fig. 1G**). These results suggest that MDK controls NR2F1 expression in melanoma cells.

Human melanoma dormant DCCs are associated with a MDK^{LOW}/$NR2F1^{HIGH}$ and $PS6^{LOW}$ phenotype.

Next, we examined the expression levels of NR2F1 and MDK in human samples from primary melanomas. We determined MDK levels in primary melanoma by IHC as shown before[5] and classify the samples into positive or negative scores as shown in **Supp. Fig. 1H**. Next, in a consecutive section, we stained with NR2F1 and HMB45 antibodies by IF (**Fig. 1D & Supp. Fig. 1I**). We observed higher signal for NR2F1 in $MDK^{negative}$ melanoma samples and lower signal for NR2F1 in $MDK^{positive}$ samples (**Fig. 1D**). Similarly, RNA obtained from three different patient-derived melanoma organoids (PDOrg) showed that patients with high levels of MDK mRNA (patient 1 (P1) and patient 3 (P3)) had lower NR2F1 levels whereas patient 2 (P2) with low levels of MDK had higher NR2F1 levels (**Supp. Fig. 1J**)).

We subsequently investigated the co-expression levels of MDK and NR2F1 in each DCC found in lymph nodes (LNs) biopsies from melanoma patients. Our analysis included LN biopsies without detectable metastasis (LN-) and another group with confirmed metastasis by standard histopathologic analysis (LN+). Notably, we observed that 30% of DCCs in LN+ samples expressed the proliferation marker Ki67, compared to only 3% in LN- samples. This finding suggests that DCCs are more likely to be in a dormant state in LN- samples (**Supp. Figure 1K**). Interestingly, we observed that ~28% of DCCs in LN- samples share the MDK^{LOW}/$NR2F1^{HIGH}$ dormant phenotype, whereas this percentage decreased to ~13% in DCCs from LN+ samples (**Fig. 1E & Supp. Fig. 1L**). By contrast, the reactivating phenotype MDK^{HIGH}/$NR2F1^{LOW}$ was higher in DCCs (~45%) from LN+ samples than DCCs from LN- samples (~14%) (**Fig. 1E & Supp. Fig. 1L**). We also observed double high and double low populations. The MDK^{LOW}/$NR2F1^{LOW}$ population represents half of the total DCCs identified in LN- samples, and since, 97% of DCCs are dormant, we can predict that this MDK^{LOW}/$NR2F1^{LOW}$ population is associated with a dormant phenotype although not through NR2F1 expression. Interestingly, MDK^{LOW}/$NR2F1^{LOW}$ population decreased to half in LN+ samples (25%, **Fig. 1E**). On the other hand, the presence of the MDK^{HIGH}/$NR2F1^{HIGH}$ population suggests that in certain DCCs MDK is not able to repress NR2F1 or that this may represent a transition phenotype from the MDK^{LOW}/$NR2F1^{HIGH}$ subpopulation towards the reactivating phenotype MDK^{HIGH}/$NR2F1^{LOW}$.

Further investigation is necessary to understand the biological significance of these double high and double low populations.

Overall, these results suggest that the shift from dormant $MDK^{LOW}/NR2F1^{HIGH}$ to reactivating $MDK^{HIGH}/NR2F1^{LOW}$ phenotype may be linked to the progression of the melanoma disease.

MDK depletion induces cell cycle arrest by upregulating NR2F1 via ALK receptor and p38 signalling.

A feature of cellular dormancy is the presence of high p38 (SAPK)/ERK (MAPK) activity ratio[11]. Thus, we calculated the phospho-p38 to phospho-ERK ratio in shControl and shMDK SK-Mel-147 cells. We showed a higher P-p38/P-ERK ratio in SK-Mel-147 shMDK when compared to the SK-Mel-147 shControl cells (**Fig. 2A**). These results suggest that downregulation of MDK may induce a quiescence phenotype. To determine whether the upregulation of NR2F1 upon MDK depletion was dependent on p38 activity, we knocked down total p38 levels by using siRNA in shMDK SK-Mel-147 cells. We observed that p38 depletion downregulated NR2F1 protein levels (**Fig. 2B**). Moreover, treatment of shControl SK-Mel-147 cells with SB203580 (a p38alpha/beta inhibitor) and TAK371 (p38alpha inhibitor) also decreased NR2F1 levels and MK2, a surrogate for p38 activity (**Fig. 2C**). The levels of SOX9, RARβ and p27, downstream targets of NR2F1, were increased in SK-Mel-147 shMDK cells when compared to shControl cells (**Fig. 2A&D**). Moreover, MDK inhibitor (iMDK) increased NR2F1, RARβ and p27 levels in SK-Mel-147 cells **(Supp. Fig. 2A**). Overall, these results suggest that MDK depletion in SK-Mel-147 MDK^{HIGH} melanoma cells upregulates NR2F1 levels and its targets downstream of p38 signalling. To determine whether MDK may have similar effects in a previously validated dormancy model, we used the dormant head and neck squamous carcinoma D-HEp3 cells[6]. We previously published that dormant D-HEp3 cells had high levels of NR2F1 when compared to the proliferative T-HEp3 cells, from which they were derived[6]. We measured MDK levels by IF and observed that proliferative T-HEp3 cells have higher percentage of MDK+ cells than D-HEp3 cells (**Supp. Fig. 2B**). Thus, the inverse correlation between MDK and NR2F1 levels also exists in the HNSCC model and the $MDK^{low}/NR2F1^{high}$ profile was associated with a dormancy phenotype. Treatment of D-HEp3 cells with rhMDK decreased NR2F1 levels (**Supp. Fig. 2C**). Next, we decided to overexpress MDK in D-HEp3 cells and determine their ability to exit dormancy using the chorionallantoic membrane (CAM) system as previously described[6] (**Supp. Fig. 2D**). We observed that exogenous expression of MDK allowed dormant D-HEp3 cells to exit dormancy and proliferate (**Supp. Fig. 2D**).

We next decided to target the anaplastic lymphoma kinase (ALK) receptor, a known binding partner of MDK, using alectinib[12-14]. We observed that alectinib-treated SK-Mel-147 cells upregulated nuclear NR2F1 protein and mRNA levels and increased phosphorylation of p38 while downregulating p-ERK and phospho-ALK when compared to control-treated cells (**Fig. 2E**). Similar results were obtained in murine B16R2L cells, which express high levels of MDK[4] (**Supp. Fig. 2E**). We then knockdown (KD) human ALK using siRNA. After confirming efficient ALK KD, we observed an increase of NR2F1 mRNA levels (2 folds) and nuclear protein levels (**Fig. 2F**).

The expression levels of NR2F1 remained unchanged when additional MDK receptors[14], specifically low-density lipoprotein receptor-related protein (LRP1), neurogenic locus notch homolog protein 2 (NOTCH2) and syndecan-3 (SDC3), were inhibited (**Sup. Fig**. **2F**).

We next measured whether MDK inhibition induces cell cycle arrest. To this end, we transduced SK-Mel-147 cells with a CDK2 biosensor (CDK2 DHB-mVenus). Here, the cytosolic to nuclear ratio of the fluorescent reporter informs whether cells are in G0/G1 (nuclear only), S (both) or G2/M phases (cytosolic only)[15]. We observed an increase (2-fold change) in the percentage of cell arrested in G0/G1 phase upon MDK depletion (**Fig. 3A**). Concomitantly, the percentage of cells in S+G2/M phases was decreased upon MDK depletion (**Supp. Fig. 3A**). We also performed cell cycle analysis by EdU incorporation and flow cytometry and showed that depletion of MDK in SK-Mel-147 cells increased the percentage of cell arrested in G0/G1 phase from ~40 to ~80% (**Fig. 3B** and **Supp. Fig. 3B**).

As an alternative method to evaluate proliferation rates in melanoma cells we used 3D Matrigel assays. We first compared the behaviour of MDK^{HIGH} vs. MDK^{LOW} in 3D cultures. We observed that, after 3 days of culture, the percentage of single cells was ~50% for WM164 and ~ 20% for SK-Mel-147 cells, arguing that WM164 cells have lower proliferation rate when compared to SK-Mel-147 cells (**Fig. 3C**). We then depleted MDK in SK-Mel-147 cells and observed that, 3 days after seeding, a higher percentage of melanoma cells remained as single cells (~25%) in shMDK group when compared to shControl cells (~12%) (**Fig. 3D**). Similarly, we observed that WM164 cells treated with rhMDK, which reduced NR2F1 levels (**Supp. Fig. 1G**), resulted in a reduction of the percentage of single cells and an increase in colonies formed after 5 days, arguing for an increase in proliferation (**Fig. 3E**).

Overall, these results showed that MDK depletion upregulates an NR2F1-dependent dormancy program via ALK and it mediates cell cycle arrest.

Activation of NR2F1 prevents melanoma metastasis by blunting the m-TOR-dependent MDK signal.

Next, we decided to evaluate the effect of an NR2F1 agonist (compound 26, C26) previously described by us[7] on dormancy associated genes in MDK^{HIGH} cells. This agonist induces NR2F1 transcriptional activity which facilitates transcription of downstream targets and itself. Treatment of MDK^{HIGH} SK-Mel-147 cells with C26 showed upregulation of NR2F1, RARB2, and p27 (**Fig. 4A**) whereas it did not change MDK secreted protein levels (**Supp. Fig. 4A**). Similar results were obtained in an additional MDK^{HIGH} melanoma cell line, SK-Mel-103 (**Supp. Fig. 4B**).

To determine the potential effect of C26 on inducing cell cycle arrest, we treated MDK^{HIGH} SK-Mel-147 3D cultures with C26 alone or in combination with the iMDK. We observed that the iMDK- and C26-treated groups had ~3-fold increase in the percentage of single cells when compared to control group and when used individually. Interestingly, the combination of both drugs increased 7-fold the percentage of single cells when

compared to control condition (**Fig. 4B**). This result led us to evaluate in a pre-clinal model whether the combination of MDK inactivity together with NR2F1 activation could serve as a potential therapeutic strategy to prevent metastasis. To this end, nude mice intravenously injected with shControl or shMDK GFP-SK-Mel-147 cells were randomly divided into vehicle or C26 treatment groups 3 days post-injection and treated for one month (**Fig. 4C**). We concluded that the number of metastatic foci in the lungs was reduced upon MDK depletion consistent with our previous results[5] and that the combination of MDK depletion plus C26 also decreased the number of metastasis when compared to control group (**Fig. 4D**). The number of metastases was reduced by treating animals injected with shControl cells with C26 alone, but this was not statistically significant. Lastly, we looked at the size of the individual foci and observed that C26 alone reduced the size of foci when compared to shControl vehicle-treated group. We also noticed that inhibition of MDK plus C26 further reduced the size of metastatic foci when compared to MDK depletion effect alone (**Fig. 4E**).

Next, we decided to analyse the phenotype of DCCs in all the *in vivo* treatments. Interestingly, analysis of the percentage of NR2F1+ DCCs, 30 days post-treatments, showed an increased in the percentage of NR2F1+ DCCs in all conditions when compared to control group (**Fig. 4F**). There were no differences in the percentages of NR2F1+ DCCs between the three treatments, however, a trend towards higher percentages of NR2F1+ DCCs was observed in MDK depletion plus C26 group (**Fig. 4F**).

To evaluate whether the use of the NR2F1 agonist alone or in combination with MDK depletion could affect survival rates, we treated animals for 28 days as in **Fig. 4C**, and measured survival rates over time. We observed that mice injected with shMDK SK-Mel-147 cells had better survival rates (90%) than control group (~60%) 26 days post-treatment (**Fig. 4G**). However, this difference disappeared at 147 days post-treatment (60% shControl+vehicle vs. 70% shMDK+vehicle) (**Fig. 4G**). Importantly, the mice injected with shMDK SK-Mel-147 cells plus C26 had higher survival rates (~90%) than shControl + vehicle and shMDK + vehicle groups at 147 days post-treatment (**Fig. 4G**). It is important to note that mice injected with shControl SK-Mel-147 cells plus C26 had a trend towards better survival rates (~80%), however, this was not statistically significant when compared to shControl+vehicle group.

To understand how the NR2F1 agonist alone or combination with MDK depletion could inhibit metastatic growth (**Fig. 4E**), we evaluated mTOR activity, previously shown to be activated by MDK in lymphatic endothelial cells[5]. In addition, we had published evidence that treatment of HNSCC DCCs with C26 in *in vitro* settings inhibited mTOR pathway[7]. Consistent with this, we observed reduced PS6 levels in SK-Mel-147 cells treated with C26 compared to control cells in vitro (**Fig. 4H**). Interestingly, the levels of PS6 in single DCCs from the lungs isolated from shControl vehicle vs. shControl C26 groups (from **Fig. 4C**) showed no significant differences (**Supp. Fig. 4C**). We hypothesized that this result might reflect the biology of dispersed DCCs in the lung epithelium, which may not be actively proliferating. However, this could change in areas where multiple DCCs are found in close proximity. To test this hypothesis, we examined lungs from the shControl vehicle group and found that only 20%

of isolated DCCs were positive for PS6 (**Fig.4I**). In contrast, in areas with clusters of more than 7 DCCs, the proportion of PS6-positive cells increased significantly to 70% (**Fig. 4I**). This suggests that clustered DCCs may be exiting dormancy and engaging in proliferation. Importantly, analysis of LN biopsies revealed that DCC clusters exhibited higher PS6 signal compared to solitary DCCs (**Fig. 4J**). These results validate in human samples our mouse findings and suggest that PS6 activation may be necessary for the transition to a proliferative state. Importantly, C26 treatment reduced the percentage of PS6+ DCC clusters compared to the vehicle control (**Fig. 4K**).

We then evaluated changes in cell cycle-related genes, known to be regulated by NR2F1[6,7], in MDK-expressing melanoma cells in response to C26 treatment. We showed previously that C26 induced upregulation of NR2F1 (**Fig. 4A**). We also observed that while rhMDK reduced the expression of p27, p21, p15, p16 and p18, the treatment with C26 induced these genes in SK-Mel-147 cells (**Supp. Fig. 4D &E**). As expected, rhMDK decreased NR2F1 levels (**Supp. Fig.4D**). Expression of the p19 gene did not respond to rhMDK nor C26 in SK-Mel 147 cells (**Supp. Fig. 4D &E)**. Similar results were obtained in SK-Mel-28 cells treated with C26, except that we observed no effect on p27 gene and upregulation of p19 upon C26 treatment (**Supp. Fig. 4F**). As shown for SK-Mel -47 cells (**Fig. 4A**), NR2F1 was also induced upon C26 treatment in SK-Mel-28 cells (**Supp. Fig. 4F**).

Combination of NR2F1 activation with MDK depletion reduced metastatic outgrowth in BRAF V600E mutant cells.

Previously studies have suggested that MDK upregulation was also overserved in cell lines carrying the oncogenic B-RAF^{V600E} mutation, which is the most frequently mutated oncogene in melanoma[16,17]. Therefore, we decided to look at NR2F1 levels in SK-Mel-28 cells, which have high levels of MDK, although not as high as SK-Mel-147 cells[5], and carry the BRAF^{V600E} mutation. Interestingly, we observed lower levels of NR2F1 in SK-Mel-28 cells when compared to SK-Mel-147 cells (**Supp. Fig. 5A**) despite having less MDK. Thus, we hypothesized that other signals besides MDK might be responsible for decreasing NR2F1 levels. We first confirmed that depletion of MDK increased NR2F1 levels (**Supp. Fig. 5B**) and that stimulation by exogenous rhMDK decreased nuclear NR2F1 intensity when compared to control group by IF (**Supp. Fig. 5C**). Next, we asked whether inhibition of BRAF^{V600E} in SK-Mel-28 cells would affect NR2F1 levels. We observed that treatment with vemurafenib (BRAF^{V600E} inhibitor) for 48 hours increased NR2F1 at the mRNA and protein levels (**Fig. 5A**), and at the same time decreased secreted MDK levels (**Supp. Fig. 5D**). We did not observe NR2F1 upregulation in SK-Mel-147 cells treated with vemurafenib (**Supp. Fig. 5E**). We also treated melanoma PDOrg carrying BRAF V600E/CDK4 R24H mutations (Patient #1) and only BRAF V600E (Patient #3) mutation with vemurafenib and observed that NR2F1 levels were induced when compared to control condition (**Supp. Fig. 5F**). Interestingly, NR2F1 targets, SOX9, RARB and p27, were also significantly induced by treatment with vemurafenib but only in Patient #3, which may be explained for higher upregulation of NR2F1 in this patient when compared to Patient #1 (**Supp. Fig. 5G**).

Next, we decided to evaluate the in vivo effect of C26 on metastasis formation in a BRAF mutant context (**Fig. 5B-D**), following the same experimental design as in **Fig. 4C**. We observed that although there was a trend towards a decrease in number of metastases in C26-, shMDK-, C26+shMDK-groups when compared to control group, the statistical analysis was not significant (**Fig. 5C**). Similarly, the size of metastases was not significantly different in C26- and shMDK-groups when compared to control group, however, we observed a decrease in sizes when mice were treated with C26 and injected with shMDK-SK-Mel-28 cells (**Fig. 5D**).

DISCUSSION

Previous studies have shown the role of MDK in favouring cancer growth, survival, angiogenesis, and the formation of distant metastasis[4,5]. However, the mechanism of action of MDK when tumor cells are lodged at secondary organs as DCCs has not been studied previously. Here, we reveal an NR2F1-driven dormancy program in melanoma DCCs that is repressed by the growth factor MDK in an autocrine manner.

In our earlier studies, we demonstrated that reducing MDK levels in the SK-Mel-147 cell line led to a decrease in lymphangiogenesis both at the primary tumor site and in lymph nodes (LN). Interestingly, this MDK reduction did not impact the formation of blood vessels[5]. Our findings reveal that depleting MDK in primary tumors does not impair dissemination of DCCs to the lungs. This observation may suggest that in this model, the spread of cancer cells to distant organs still occur through blood vessels when lymphangiogenesis is dysfunctional. Further investigation on this regard is needed to decipher the mechanisms of dissemination of melanoma cells to distant sites.

MDK is a secreted cytokine which could travel to distant sites, perhaps in exosomes, from the primary tumor as we previously shown[5]. In this study, we have used tail vein injection to eliminate the effect of a pre-metastatic niche created by the primary tumor. Nevertheless, we still observed the lack of metastatic capacity of melanoma cells depleted of MDK. This result suggests that the autocrine MDK activity could be enough to trigger metastatic outgrowth of DCCs, as depletion of MDK in DCCs impaired metastasis formation.

Our previous research has generated promising results in preventing metastasis formation using the NR2F1 agonist C26 in a pre-clinical model of head and neck squamous cell carcinoma (HNSCC)[7]. This success lends support to the concept that therapies aimed at inducing dormancy could be advantageous in certain types of cancer. A particularly noteworthy finding emerged in this work when we administered C26 to mice harboring MDK^{HIGH} disseminated cancer cells (DCCs) with a BRAF wild-type background. While the treatment did not significantly alter the number of metastatic sites, it resulted in a marked reduction in the size of metastatic lesions (**Fig. 4**). This suggests that activating NR2F1 with C26 may hinder the growth of metastases during the early phases of DCC reawakening. This observation aligns with our findings in human LN DCCs (**Fig. 4**), which may indicate activation of the mTOR pathway during the transition from single DCC to small clusters of DCCs. Importantly, C26 appears to reduce the mTOR activation in clusters of DCCs. These results are particularly

significant as they pave the way for investigating the potential use of mTOR inhibitors, either alone or in combination with C26, to prevent the reactivation of MDK^{HIGH} DCCs in melanoma patients. Noteworthy, new clinical trials in breast cancer patients are testing whether combining autophagy and mTOR inhibitors can target dormant DCCs and prevent late recurrence (CLEVER pilot trial, NCT03032406).

Our study revealed that approximately 80% of animals injected with MDK^{HIGH}/BRAF wild-type SK-Mel-147 cells and treated with C26 alone for one month remained disease-free after 5 months post-treatment, compared to the control group. However, this difference was not statistically significant. Notably, only the combination of MDK depletion and C26 treatment significantly improved survival rates. This data may become critical for translational research in where the design of a treatment for melanoma patients carrying high levels of MDK will imply to not only stop the pro-tumorigenic signal driven by MDK but also enforce NR2F1 activation. Previous studies have shown the development of nanoparticles containing mRNA against MDK that successfully work in pre-clinical models of hepatocellular carcinomas[18]. Therefore, a combination of anti-MDK nanoparticles and the NR2F1 agonist could potentially serve as a therapeutic strategy to prevent metastasis in MDK^{HIGH} melanomas.

In vivo experiments using MDK^{HIGH}/$BRAF^{V600E}$ SK-Mel-28 cells showed that only the combination of MDK depletion and C26 treatment significantly reduced metastasis size compared to the control. Interestingly, C26 alone did not statistically decrease the number or size of metastases in these cells. This may be explained by the activated BRAF signaling blocking NR2F1 expression (**Fig. 5 and Supp. Fig. 5**). In this scenario, combining BRAF mutant inhibitors with C26 may be a more effective strategy to extend survival in patients with MDK^{HIGH}/BRAFV600E melanomas. Finally, since inactivation of mutant BRAF also led to upregulation of NR2F1, these results suggest that inducing dormancy by activating NR2F1 could be an opportunity to overcome de novo vemurafenib resistance observed in patients diagnosed with MDK^{HIGH}/BRAFV600E melanoma.

In patients diagnosed with melanoma, the presence of a limited number of DCCs in LN- has been reported, and their presence is associated with increased risk for death when compared to patients without DCC detection[1,2]. However, the removal of sentinel lymph nodes does not extend overall survival of patients with melanoma, suggesting that DCCs in other organs may play important roles in survival rates. Since DCCs found in LNs can predict systemic cancer progression[1,2], the analysis of LN DCC sub-populations based on phenotype may reflect DCC phenotypes in other organs and be relevant for prognostic information. Using the same HMB45 antibody as previously described to identify single DCCs in LNs[1,2], we conclude that there is an association between higher percentages of reactivating MDK^{HIGH}/$NR2F1^{LOW}$ DCCs in LN+ for metastases and higher percentages of dormant MDK^{LOW}/$NR2F1^{HIGH}$ DCCs in LN- for metastases. From a translational perspective, these findings could be validated in LN biopsies collected at the time of melanoma diagnosis with follow up data on date of recurrence and/or death. In this regard, our analysis of a small cohort of patients shows that 3 out of 3 patients carrying a dominant dormant MDK^{LOW}/$NR2F1^{HIGH}$ DCC population, remain alive 20 years later. On the other side, 2 out of 3 patients carrying a dominant reactivating MDK^{HIGH}/$NR2F1^{LOW}$ DCC population, were deceased in less than 3

years. Increasing the number of patient samples will confirm whether higher percentages of reactivating $MDK^{HIGH}/NR2F1^{LOW}$ DCCs may predict for higher risk of recurrence.

In recent years, our research has demonstrated the role of MDK in modulating both innate and adaptive immune cells, using murine B16-derived cells in immunocompetent animals[4]. While our current study using athymic mice limits our ability to investigate immune system interactions, our previous work has shown that NR2F1 can induce dormancy similarly in both immunosuppressed and immune-competent mice. This has been demonstrated in models such us MMTV-myc[6] and MMTV-PyMT[19] mouse models. Although outside of the scope of this manuscript, future plans will involve the study of immune cues regulated by the NR2F1-driven dormancy program in murine melanoma models.

This research exposes a gap in our understanding of melanoma progression, revealing that certain melanomas are less prone to DCCs becoming dormant before any treatment is applied. Our results show for the first time an interplay between MDK cytokine and the dormancy inducer NR2F1 in lung melanoma DCCs during dormancy. Our results also offer different strategies to prevent melanoma DCC reactivation and maintain longer periods of remission.

Acknowledgements

We extend our sincere gratitude to all the members of the Sosa's lab including rotation PhD. student Subramanian Thothathri. We also acknowledge Ahron Flowers and the Tara Miller Melanoma Center at University of Pennsylvania for the melanoma specimens. We would also like to specially acknowledge Dr. Julio Aguirre-Ghiso for his persistent guidance and the invaluable contributions of his lab members, whose thoughtful discussions during our weekly meetings significantly enriched our research process. We acknowledge Jinghang Zhang from the Flow Cytometry Core and Hillary Guzik at the Analytical Imaging Facility at the Albert Einstein College of Medicine (with support from the NCI Cancer Center Support Grant P30CA013330) for training on the use of The Cytek® Aurora and Hamamatsu S60 slide scanner, respectively. Grant support: MRA Team Science Award N401181 (M.S.Soengas and M.S.Sosa); Gilead Research Scholars (M.S.Sosa.); MRF-CDA (M.S.Sosa).

Author Contributions

C.R-T. designed, performed in vitro and in vivo experiments, collected microscopy data, analysed data and co-edited the manuscript; T.A.R. performed IF, WB, qPCR experiments, expanded patient-derived melanoma organoids and analysed data; A.A.R. performed 3D, IF, WB, qPCR experiments and analysed data; N.K. IF, WB, qPCR performed experiments and analysed data; S.J.S. performed IF, WB, qPCR experiments and analysed data; A.P-G. performed CDK2 reporter experiments and analysed data; D.O. provided reagents and edited the manuscript; M.S.Soengas provided reagents and edited the manuscript, M.S.Sosa designed and executed CAM assays and in vivo experiments, provided general oversight, collected microscopy data, analysed data and wrote the manuscript.

MATERIALS AND METHODS

Cell lines

Highly metastatic GFP-SK-Mel-147 cells, SK-Mel-28, WM164 and B16R2L cells were obtained from Dr. Maria S. Soengas laboratory at CNIO, Spain. SK-Mel-103 cells were obtained from Dr. Eva Hernando laboratory at NYU, USA. Cells were cultured in DMEM (Dulbecco's modified medium, Corning 10-031-CV)) supplemented with 10% V/V FBS and 100 U penicillin/ 10 mg/mL streptomycin (Life science # 30-002-CI).

T-HEp3 cells were derived from a lymph node metastasis from a HNSCC patient as described previously[20] and kept as PDXs on chick chorioallantoic membrane (CAM). D-HEp3 cells were obtained by passing T-HEp3 cells for more than 40 generations in vitro[20]. In vitro, these cells were cultured in DMEM with 10% of FBS, 100 U/mL penicillin and 0.1 mg/mL streptomycin.

Transfection

D-HEp3 cells were transfected with ORF lentiviral expression vector pReceiver-Lv105-A0792 (pEX-MDK) and the corresponding empty vector (pEX-Neg) plasmid (obtained from Dr. Maria S. Soengas laboratory at CNIO) by using Fugene6 (Promega) in serum free and antibiotic-free media according to the manufacturer's instructions.

Transient knockdown experiments were done using small interfering (si)RNA. Cells were seeded at a density of 20,000 cells/cm^2 and allowed to reach 60-70% confluency. Cells were then transfected using Lipofectamine™ RNAiMax (Thermo Fisher # 13778150) in serum free media following manufacturer's instructions. Media was changed 12 h later and incubated for a total of 48 h before analysis. siRNAs were used at 50 nM unless otherwise specified. For ALK knockdown, cells were transfected with 30 nM ON-TARGETplus Human ALK (238) siRNA - SMARTpool (Horizon # L-003103-00-0005) in serum free and antibiotic-free media according to the manufacturer's instructions. ON-TARGETplus Non-targeting Control Pool (Horizon # D-001810-10-05) was used as a control.

Cell cycle analysis

Cell cycle was determined by flow cytometry after EdU (5-ethynyl-2 deoxyuridine) incorporation. For this, cells were incubated with 10uM Edu in full media, for 1 h, immediately before collection. Cells were lifted, washed in serum free media, and stained with Zombie NIR for 15 at room temperature. Cells were washed and fixed on 4% w/v in PBS for 20 min on ice. Edu was detected by Click-iT™ Edu Alexa Fluor™ 647 kit (Thermo Fisher # C10634) following manufacturer's instruction. EdU and DNA content (DAPI staining) was determined on a Cytek Aurora Analyzer at the Flow Cytometry Core Facility at the Albert Einstein College of Medicine. Data was analyzed using FlowJo software.

Cell carrying the CDK2-mVenus reporter (Addgene #136461) were processed for IF. As the CDK2 mediated phosphorylation of this reporter leads to a conformational change that causes the reporter to translocate from the nucleus to the cytoplasm, the ratio of cytoplasmatic to nuclear fluorescence indicates G0/G1 (nuclear only), S (both) or G2/M phases (cytosolic only) were calculated. Images were subjected to cell segmentation using DAPI signal to determine nuclear area and a 2 um expansion to determine cytosolic signal using QuPath software. Cell cycle stage was determined by calculating the cytosolic/nuclear ratio of the mean mVenus fluorescence as previously described[15].

Lentiviral transduction

293T cells were seeded at 35,000 cells/cm^2 in full DMEM media. Once cultures reached 80% confluency, they were transfected with 2.5 µg of lentiviral vectors using Lenti-pack HIV Expression Packaging Kit (GeneCopoeia # LT001) in serum free media. Cell culture media was replaced with full media supplemented with Titerboost™ reagent (1:500 dilution) 12 hours after transfection. Supernatants enriched in viral particles were collected 48 h and 72 h later. Pooled supernatants was filtered through a 0.45-µM filter and concentrated using Lenti-X concentrator (Takara # 631231). Aliquots were used immediately or stored at -80C for 6 months.

To generate stable cell lines, SK-Mel-147 and SK-Mel-28 cells were transduced with lentiviral particles carrying CDK-DHB-mVenus[15], shControl or shMDK constructs in full media supplemented with 0.8 µL/mL Polybrene (EMD Millipore # TR-1003-G). Cell culture media was replaced 24 h after, and selection of transduced cells was carried by treatment with 1ug/ml puromycin 72 h post-infection. Targeting/non targeting sequences were obtained from Dr. Maria S. Soengas (shMDK#5 NM_002391.3-621s21c1 5'-CCGGTGTCTGCTCGTTAGCTTTAATCTCGAGATTAAAGCTAACGAGCAGACATTTTTG-3'; shMDK#1 NM_002391.3-505s21c1 5'-CCGGAGGGAAGGGAAAGGACTAGACCTCGAGGTCTAGTCCTTTCCCTTCCCTTTTTTG -3'; shControl CAACAAGATGAAGAGCACCAA).

CAM assays

Tumor growth of T-HEp3 cells on CAM has been already described[21]. Briefly, Control or ORF-MDK D-HEp3 cells were inoculated on CAM and allowed to grow for 7 days. Tumors were harvested and digested with collagenase 1A (Sigma-Aldrich; C9891) for 30 min at 37°C. T-HEp3 tumor cells (recognized by their very large size compared with chicken cells) were counted using a hemacytometer.

Animal models

Animal procedures were approved by the Institutional Animal Care and Use Committee (IACUC) of Icahn School of Medicine at Mount Sinai with protocol 2017-0162, and the Albert Einstein College of Medicine with protocol

00001676. Nude mice were purchased from Jackson Laboratories (Stock #002019) and maintained under SPF conditions throughout the experiment.

To determine metastatic burden after knockdown of MDK, nude female animals of 6 weeks of age were intravenously injected with shControl or shMDK SK-Mel-147 cells. Cells had been expanded, collected at 80% confluency, and single cells resuspended in 1X PBS. Animals were injected with 100 uL of cell suspension (10,000 cells/mouse) on the tail vein using a 27G needle. Twenty-one days later, mice were euthanized, and lungs were collected after perfusion. Animals were maintained under SPF conditions throughout the experiment and monitored twice weekly.

To determine the effect of C26 on metastatic burden, nude female animals of 6 weeks of age were intravenously injected with shControl or shMDK cells ($1x10^6$ cells/mouse in 100uL) on the tail vein using a 27G needle. Three days after injection, animals started treatment with C26 (0.5mg/Kg) or vehicle (30% v/v PEG300, 5% v/v Tween80 and 4% v/v DMSO in sterile water) by intraperitoneal injection every other day, for 28 days. Animals were maintained under SPF conditions throughout the experiment and monitored thrice weekly. Twenty-eight days later, mice were euthanized, and lungs were collected after perfusion.

Patient Samples

Paraffin embedded sections from patient melanoma tumors and lymph nodes (positive and negative for metastasis by histopathological analysis) were obtained from Dr. Lynn Schuchter from the University of Pennsylvania (MTA ID: 44613/00, MTA ID:000344-2025). Patient derived organoid (PDOrg) models were expanded obtained from the NCI Patient Derived Models Repository (NCI PDMR; Frederick, MD; https://pdmr.cancer.gov) and expanded by the Dr. Emily Bernstein's Laboratory (Mount Sinai, NY). Patient 1 (P1): 425362 [Lot# 425362-245-T-V1-organoid]; Patient 2 (P2): 875164 [Lot# 875164-322-T-V2-organoid]; Patient 3 (P3): 251568 [Lot# 251568-266-R-V1-organoid].

3D cultures

WM164 cells were grown in 3D cultures in 8-well chambers (Corning # 354118). For this, 8 well chambers were coated with a layer of growth factor reduced Matrigel® (Corning # 354230). After Matrigel® was solid, 1,000 cells were seeded on top, in complete media and allowed to form colonies for 48 h. Then, cells were treated with vehicle or 20 ng/mL recombinant human Midkine rhMDK for 48 h. Brightfield images were taken on Leica DMi8 scope (20X, DIC) daily. On day 5, cells were fixed using 4% w/v PFA for 20 min at room temperature and process for immunofluorescence.

SK-Mel 147 shControl cells pretreated with 1uM Compound 26[7] and 25nM MDKi (EMD Millipore # 508052) for 48hrs in 2D. Cells were then seeded in 8 well chambers (1000 cells/well) over a layer of Matrigel and maintained

treatment with C26, MDKi, or a combination of both drugs for 6 days. Brightfield images were taken daily on a Zeiss Axio Observer scope (20X, DIC).

Patient-derived organoids (PDOrg) were grown as organoids embedded in 3D Cultrex™ basement membrane extract (BME) (R&D Systems # 3533-005-02). Four thousand cells were seeded in 35uL domes of BME in 24 well plates. BME was allowed to harden at 37°C for 30 min. After that, 750uL of complete feeding media [(1X Advanced DMEM/F12 (Invitrogen # 12634-028), 10 mM HEPES (Invitrogen # 15630080), 1X GlutaMax Supplement (Life Technologies # 35050061), 0.1 mg/mL Primocin (InvivoGen # Ant-pm-2), 1.25 mM N-acetylcysteine (Sigma # A9165-5G), 50% V/V L-WRN Conditioned Media, 10 mM Nicotinamide (Sigma # N0636-100G), 1X N21-MAX Media Supplement (R&D Systems # AR008), 10uM Y-27632 dihydrochloride (Tocris # 1254),1X N-2 MAX Media Supplement (R&D Systems # AR009)] was added to each well. Cells were collected by using 750ul/well splitting media [1X Advanced DMEM/F12 (Invitrogen # 12634-028), 10 mM HEPES (Invitrogen # 15630080), 1X GlutaMax Supplement (Life Technologies # 35050061), 0.1 mg/mL Primocin (InvivoGen # Ant-pm-2), 2.5% V/V FBS, 1.5mg/mL Dispase II (ThermoFisher Scientific, #: 17105-041)] for 2 hr at 37C. After that, cells were collected by centrifugation and RNA extraction was done by using RNeasy Micro Kit (Qiagen # 74004).

Western blot

Whole cell lysates were obtained from SK-Mel-147 shControl and shMDK cells grown at 70-80% confluency and serum-starved for 20 hours. Samples were collected in 1xRIPA buffer and centrifuged at 12000rpm and 4°C to clarify lysates. Cell fractionated lysates were obtained from cells seeded at a density of 36,000 cells/cm2 and treated with P38 inhibitor SB203580 (Sellechem # S1076) or MDK inhibitor iMDK (EMD Millipore # 508052) in serum-free medium for 24 hours. To test the responses to Alecitinib treatment, SK-Mel-147 parental cells were treated with 0.5 uM or 1 uM Alecitinib in full media for 24 h. Cells were washed once with cold 1X-PBS and processed for nuclear and cytosolic protein fractionation using a cytoplasmic and nuclear protein extraction kit (Boster bio # AR0106). Protein concentration was determined using BCA protein assay kit (Pierce #23227) and a standard BSA curve. Samples were then boiled for 5 min at 95°C in SDS-Page sample loading buffer (Bioscience # 786-701). SDS-PAGE gels at 8 or 10% were run in Running Buffer (25mM Tris, 190mM glycine, 0.1% w/v SDS) and transferred to PVDF membranes in Transfer Buffer (25mM Tris, 190mM glycine, 20% v/v methanol). Membranes were then blocked in 5% w/v milk in TBST (Tween20-TBS buffer; 50mM Tris, 150mM Sodium Chloride, 0.1% Tween20®, pH7.6). Membranes were incubated in primary antibodies at 4°C overnight. Following 3 washes with TBST buffer, membranes were incubated with HRP-conjugated secondary antibodies at room temperature for one hour. Western blot development was done using Amersham ECL Western Blot Detection (GE, RPN 2106) and GE ImageQuant LAS 4010.

Immunofluorescence staining

Cells in 2D cultures (SK-Mel 147 shC, shMDK and Wm164 cells) were seeded on 12mm coverslip and, after 24 h, fixed with 4% w/v PFA. Cells were permeabilized using 0.1% v/v Triton X-100 in PBS for 20min, treated with 50mM NH_4Cl, and blocked using 3% BSA in PBS + 10% Normal Goat Serum (Gibco #PCN5000) for one hour. Coverslips were then incubated with primary antibodies for MDK and NR2F1 overnight at 4C. Secondary antibodies were used at 1:1000 dilution in 3% w/v BSA in PBS. Coverslips were mounted with ProLong™ Gold Antifade reagent with DAPI (Invitrogen #P36931).

Lymph node and primary tumors sections from 10 patients were stained using Multiplexed Immunohistochemical consecutive staining in a single slide (MICSSS)[22] using antibodies against human Midkine, NR2F1 and HMB45. For this, sections were baked overnight at 60C and deparaffinized and rehydrated by consecutive xylene and ethanol washes. Heat-induced antigen retrieval was done for 30 min at pH6 with a 10mM citrate buffer. Slices were rinsed with TBS (10mM Trizma, 150mM NaCl, pH7.4) and permeabilized at RT for 5 min in 0.1% v/v Triton X100 in TBS. Endogenous peroxidase was quenched by incubation in 3% H_2O_2 for 15 min at room temperature before blocking with SuperBlock (Thermo Fisher #37515) for 30 min. Tissues were then incubated with an anti-HMB45 antibody diluted in TBS at 4ºC overnight, washed in 0.04% v/v Tween 20 in TBS for 5 min and incubated with HRP-conjugated secondary antibodies at 1:500 dilution in TBS for 1 h at room temperature. Slides were developed using AEC solution following manufacturer's instruction (Vector # SK-4200), counterstained with Harris hematoxylin, and mounted in Glycergel (Dako # C056330). Sections were imaged using the Hamamatsu Slide Scanner S60 at a 20X magnification. Then, sections were subjected to consecutive rounds of demounting, destaining, re-staining and imaging. For demounting, sections were incubated in warm water (55ºC) until coverslips slipped off on its own and washed in water. For destaining, sections were immersed in 50% v/v ethanol for 2 min, 1.2N HCL in 70% v/v ethanol for 2 min, 100% v/v ethanol for 5 min, 70% v/v ethanol for 2 min, 50% v/v ethanol for 2 min, and water for 5 min. Slides were monitored at this step to confirm destaining of AEC and hematoxylin by microscopy. Slides were then subjected to a second round of antigen retrieval for 10 min at pH6 with a 10mM citrate buffer or at pH9 using a Tris-based solution (Dako # H-3301), depending on primary antibody. Blocking with Fab fragments (Jackson ImmunoResearch #715-007, #711-007, or #712-007) inTBS was followed by primary and secondary antibody staining, development, mounting and imaging. As a last round, sections were processed for fluorescent staining with antibodies against HMB45, phosphoS6 and Ki67, using Hoechst 33342 (Thermo Fisher #H3570) as counterstaining. All images were acquired using a Hamamatsu S60 Nanozoomer scanner (Analytical Imaging Facility, Albert Einstein College of Medicine), stacked and aligned using the Linear stack alignment with SIFT plugin in FIJI (ImageJ). HMB45+ regions were annotated using QuPath and classified as DCCs (single cell), small clusters (between 2 and 10 cells), micromets (between 11 and 100 cells) and macromets (above 100 cells). These regions were then scored based on MDK and NR2F1 staining. Cell segmentation over Hoechst 33342 signal (nuclear area) and cell expansion of 2um (cytosol) were used to determine the mean fluorescence signal of Ki67 and pS6, respectively.

Mouse tissue sections were deparaffinized and rehydrated as before. Antigen retrieval was done in 10 mM sodium citrate buffer (pH 6) and permeabilized in 0.1% v/vTriton x-100 in PBS. Blocking was done using 3% w/v BSA in PBS with 1.5% v/v normal goat (MP Biomedicals #8642921) or normal donkey serum (Sigma-Aldrich #D9663; RRID:AB_2810235). Primary antibodies at 1:100 dilution unless otherwise specified–were used overnight at 4ºC. Secondary antibodies at 1:1000 dilution were assessed for 1 hour at room temperature. Slides were mounted using Prolong Gold Antifade mounting media with DAPI (Molecular Probes #P36931). Image acquisition was done using Leica DMi8 fluorescence microscope and image processing was done using LAS X Leica software and FIJI software.

qRT-PCR

RNA was extracted from 2D and 3D cell cultures using Trizol™ (Thermo Fisher # 15596026) or using Qiagen Micro RNeasy columns (Qiagen #74004). RNA (1-2 ug) was treated with DNase I (Thermo Fisher # AM2222) and retrotranscribed using RevertAid First Strand cDNA Synthesis Kit (Thermo Fisher #K1622). Quantitative real time-PCR was performed using PerfeCTa SYBR® green FastMix(R) Reaction mix (Quantabio #95072) in Agilent QuantStudio3. *Tubulin* was used as housekeeping control for all plates and gene expression determined using the ΔΔCt method.

Statistical Analysis. Statistical analysis was done using Prism Software. Differences were considered significant if *P* values were <0.05. For the majority of cell culture experiments, unless specified otherwise, one tailed *student t-tests* was used. For mouse experiments one tailed *Mann-Whitney* tests was used. Chosen sample size was determined empirically.

Reagents lists

Table 1: qRT-PCR primers

Target Gene	Primer ID	Sequence
hMDK	MDK-F	5'-CCTGCAACTGGAAGAAGGAG -3'
	MDK-R	3'-CTGGCACTGAGCATTGTAGC-5'
hNR2F1	NR2F1-F	5′- CCAATACTGCCGCCTCAA -3′
	NR2F1-R	5′- GGTTGGAGGCATTCTTCCTC -3′
hSOX9	SOX9-F	5′-CACTCCTCCTCCGGCATG-3′
	SOX9-R	5′-GGCTGCACGTCGGTTTTGG-3′
hRARβ	RARβ-F	5′-GTACCACTATGGGGTCAGCG-3′
	RARβ-R	5′-CGACAGTATTGGCATCGATTCC-3′
hTubulin	Tubulin-F	5′-CCCTCCAAGCTCTACTCT-3′
	Tubulin-R	5′-GACCAAGGCTGGTCTCTTTC-3′.
hp27	p27-F	5′- GGTTAGCGGAGCAATGCGCA -3′

	p27-R	5′ -AACCGGCATTTGGGGAACCGTC -3′.
hNOTCH2	NOTCH2-F	5′ -TGCCCTAACCACAGGTGTCA-3′.
	NOTCH2-R	5′ -CCCATTTTGACAGGCATTGGG-3′.
hLRP1	LRP1-F	5′ -CGGGCCTTCGTTTTGGACG-3′.
	LRP1-R	5′ -AGGGTCAGGACATTGGCTCC-3′.
hPTPRZ1	PTPRZ1-F	5′ - ACTCATGCCCTCTCTGGTGA-3′.
	PTPRZ1-R	5′ - TGTCAGCCCATCTGTGTCAG-3′.
hSDC3	SDC3-F	5′-TGACATCCCTGAGAGGAGCA-3′
	SDC3-R	5′-AAGGTCTCTGGAGTTGGGGT-3′
hCCND1	CCND1-F	5′ -GGCTTTCTCTGATGTAATTCTTGC-3′
	CCND1-R	5′ -GTATTTTGGTCTGACTGCTTGC-3′
hCDKN1B- p27	CDKN1B- p27-F	5′ -GGTTAGCGGAGCAATGCGCA-3′
	CDKN1B- p27-R	5′ -AACCGGCATTTGGGGAACCGTC-3′
hCDKN1A-p21	CDKN1A-p21-F	5′ -TGCCGAAGTCAGTTCCTTGT-3′
	CDKN1A-p21-R	5′ -GTTCTGACATGGCGCCTCC-3′
hCDKN2B-p15	CDKN2B-p15-F	5′ -GGGACTAGTGGAGAAGGTGC-3′
	CDKN2B-p15-R	5′ -CCATCATCATGACCTGGATCG-3′
hCDKN2A-p16	CDKN2A-p16-F	5′ -GGGGTCGGGTAGAGGAGG-3′
	CDKN2A-p16-R	5′ -GCCCATCATCATGACCTGGA-3′
hCDKN2C-p18	CDKN2C-p18-F	5′ -GGGCGGGTTTTTCAACTCAA-3′
	CDKN2C-p18-R	5′ -GTGCCGGTTTCTTCTCCCTT-3′
hCDKN2D-p19	CDKN2D-p19-F	5′ -CATGCTGCTGGAGGAGGTTC-3′
	CDKN2D-p19-R	5′ -CATGCTGCTGGAGGAGGTTC-3′
hALK	ALK-F	5′ -GGATGGCCCGAGACATCTAC-3′
	ALK-R	5′ -AGCACTCCAAAGGACCATGT-3′

Table 2: siRNA targeting sequences

Target gene	Manufacturer	Reference Number	Sequence
MDK	Sigma Aldrich	SASI_Hs01_00172412	5’-GGACUAGACGCCAAGCCUG-3′
NR2F1#1	Sigma Aldrich	SASI_Hs01_00095428	5’-AACAUAUCGCGGAUGAGAG-3′
NR2F1#2	Sigma Aldrich	SASI_Hs01_00095429	5’-CCGUCAUCGAGCAGCUCUU-3′
SDC3	Sigma Aldrich	SASI_Hs02_00345983	5’-CUGAUUGGCUGGUGGUGGA-3′
NOTCH2	Sigma Aldrich	SASI_Hs01_00068802	5’-GAGUUAUACUUGCUUGUGU-3′
LRP1	Sigma Aldrich	SASI_Hs01_00104587	5’-CAUCGAUCUUCACAAAGGA-3′
PTPRZ1	Sigma Aldrich	SASI_Hs01_00144476	5’-AAUCAUGCACAGGUAUUGC-3′

Table 3: Antibody list

Antibody Name	Manufacturer	Catalog Number	RRID	Use
NR2F1	Abcam	181137	AB_2890250	WB (1:300) IF (1:100) MICSSS (1:100)
SOX9	Millipore	AB5535	AB_2239761	
p27	CST	3686	AB_2077850	IF (1:100)

phospho-P38	CST	9211S	AB_331641	WB (1:1000)
P38	CST	9212	AB_330713	WB (1:1000)
phospho-ERK 1/2	CST	9106	AB_331768	WB (1:1000)
ERK 1/2	CST	9102	AB_330744	WB (1:1000)
B-Tubulin	Abcam	Ab15568	AB_2210952	WB (1:1000)
GAPDH	CST	2118	AB_561053	WB (1:1000)
Lamin B1	CST	12586S	AB_2650517	WB (1:500)
p-AKT	CST	4060s	AB_2315049	WB (2:1000)
AKT	CST	4685s	AB_2225340	WB (1:1000)
p-ALK	CST	3341s	AB_331047	WB (2:1000)
p-ERK	CST	4377s	AB_331775	WB (1:1000)
ALK	CST	3633	AB_11127207	WB (1:1000)
MK-9 (MDK)	Santa Cruz	sc-46701	AB_627949	IF (1:50) MICSSS (1:50)
HMB45	Santa Cruz	sc-59305	AB_784471	IF (1:50) MICSSS (1:100)
Vimentin	R&D	MAB21051	AB_2216114	IF (1:100)
ATF2	CST	35031	AB_2799069	WB (1:1000)
Phospho-ATF2	Abcam	ab32019	AB_725567	WB (1:500)
MK2	CST	3042	AB_10694238	WB (1:1000)
p-MK2	CST	3041	AB_330726	WB (1:1000)
RARβ				
β-Actin	CST	3700	AB_2242334	WB (1:1000)
Phospho-S6	CST	5364	AB_10694233	WB (2:5000) IF (1:150)
S6	CST	2217	AB_331355	WB (2:5000
AF488 anti-mouse	Thermo	A-11001	AB_2534069	IF (1:1000)
AF568 anti- rabbit	Thermo	A-11036	AB_10563566	IF (1:1000)
Ki67-APC	Miltenyi	130-120-556	AB_2784389	IF (1:150)
AF488 anti-goat	Thermo	A11055	AB_2534102	IF (1:1000)
AF647 anti-rabbit	Thermo	A-31573	AB_2536183	IF (1:1000)

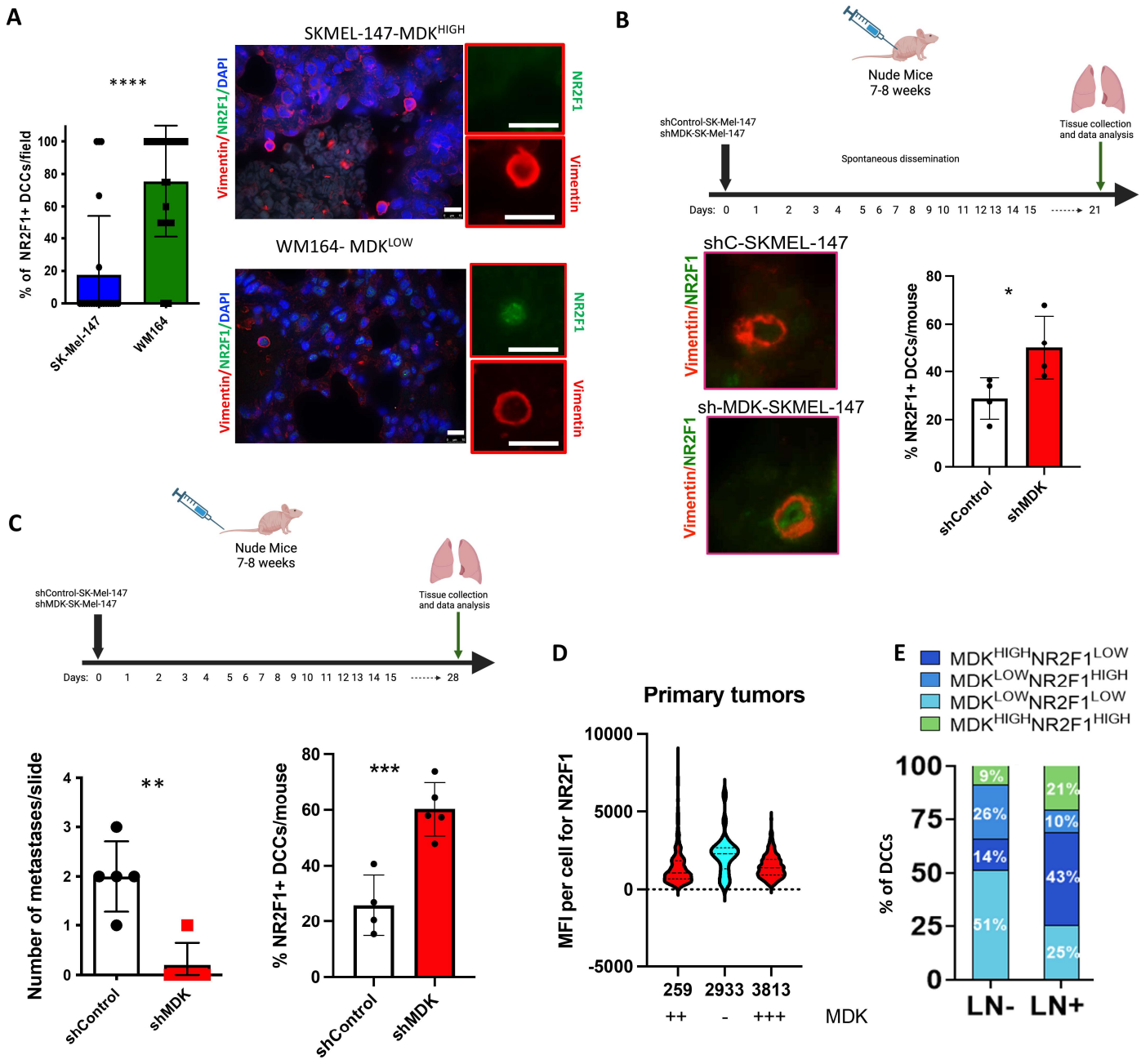

Figure 1. High levels of MDK are associated with low levels of NR2F1 in melanoma. A. SK-Mel-147 (SK) and WM164 (WM) cells were s.c. injected into nude mice. Lung sections were stained for NR2F1 (green), human vimentin (red, recognizes only human vimentin) and DAPI (blue). Zoom in pictures show single DCCs. 10 µm scale bars (white bars). Bar plots show percentage of NR2F1+ DCCs/field. Mann-Whitney test. **B.** GFP-SK-Mel-147 (shControl and shMDK) cells were implanted s.c. in nude mice. Lungs were collected 21 days later and embedded in paraffin. Lung sections were stained for NR2F1 (green), Vimentin (red) and DAPI (Blue). Percentage of NR2F1+ DCCs/mouse in lungs injected with shControl- or shMDK-SK-Mel-147 (two shRNAs against MDK) cells. Mann-Whitney test. **C.** shControl and shMDK GFP-SK-Mel-147 cells (10,000 cells/mouse)

were i.v. injected in nude mice. Lungs were collected and embedded in paraffin. Number of metastasis was determined on H&E stained sections and the percentage of NR2F1+ DCCs/mouse was determined after IF. Mann-Whitney test. **D.** Primary tumors were scored for MDK based on IHC staining (**Suppl. Fig. 1**, ++=intermediate, +++= high, -= negative). Sequential sections for each tumor were stained for NR2F1 and HMB45. NR2F1 mean fluorescent intensity (MFI) per nuclei was plotted. Numbers on x axis represent deidentified patients. **E.** Lymph nodes carrying metastasis (LN+, N=7 patients, number of DCCs analyzed:106) vs. LN without apparent metastasis (LN-, N=4 patients, number of DCCs analyzed:35) were used to identify single DCCs and determine the percentages of DCCs with the indicated phenotypes among patients.

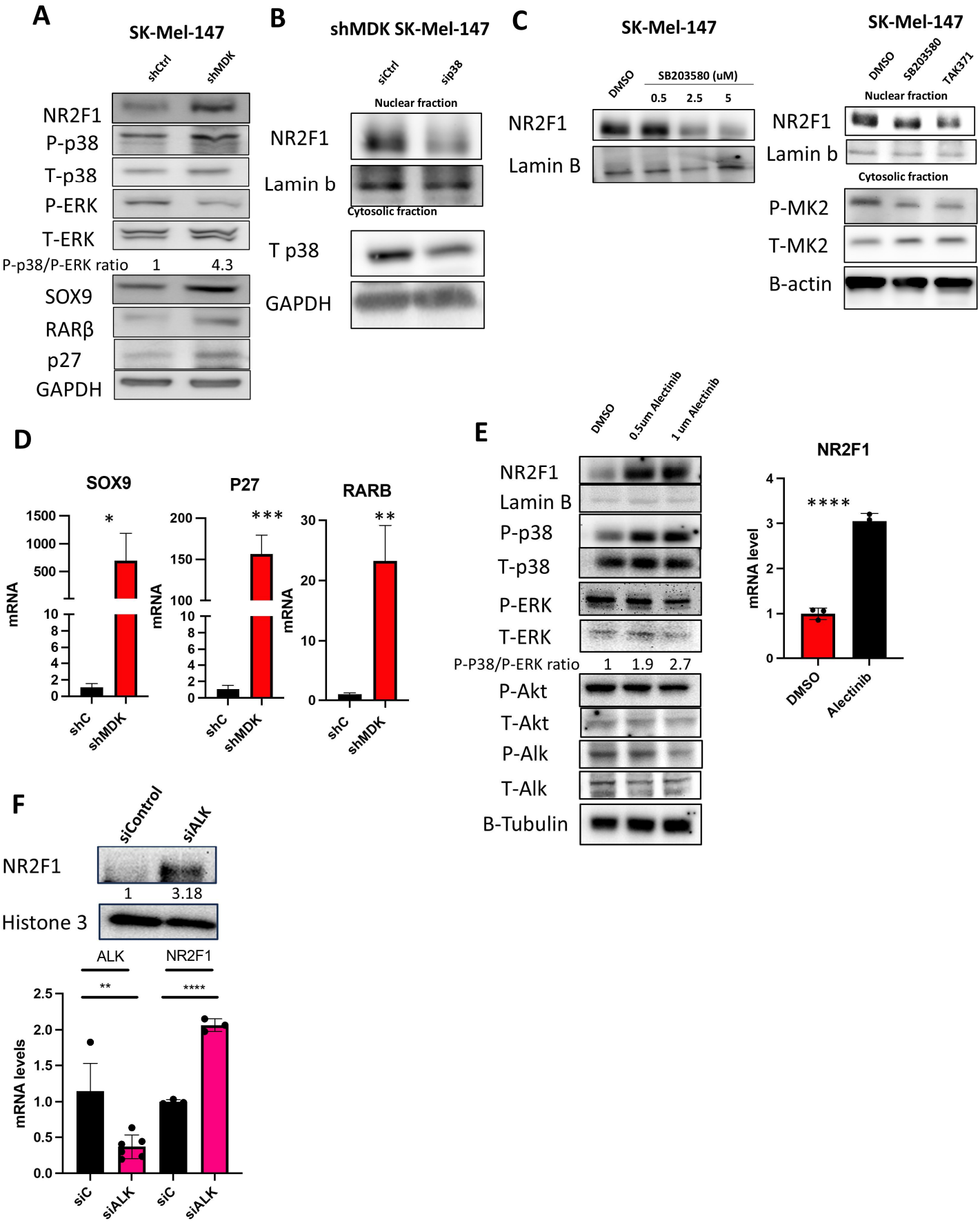
A
SK-Mel-147
shCtrl
shMDK
NR2F1
P-p38
T-p38
P-ERK
T-ERK
P-p38/P-ERK ratio 1 4.3
SOX9
RARβ
p27
GAPDH
B
shMDK SK-Mel-147
siCtrl
sip38
Nuclear fraction
NR2F1
Lamin b
Cytosolic fraction
T p38
GAPDH
C
SK-Mel-147
DMSO
SB203580 (uM)
0.5 2.5 5
NR2F1
Lamin B
SK-Mel-147
DMSO
SB203580
TAK371
Nuclear fraction
NR2F1
Lamin b
Cytosolic fraction
P-MK2
T-MK2
B-actin
D
SOX9
P27
RARB
mRNA
shC
shMDK
E
DMSO
0.5um Alectinib
1 um Alectinib
NR2F1
Lamin B
P-p38
T-p38
P-ERK
T-ERK
P-P38/P-ERK ratio 1 1.9 2.7
P-Akt
T-Akt
P-Alk
T-Alk
B-Tubulin
NR2F1
mRNA level
DMSO
Alectinib
F
siControl
siALK
NR2F1
1 3.18
Histone 3
ALK
NR2F1
mRNA levels
siC
siALK

Figure 2. Midkine depletion induces expression of NR2F1 and its downstream targets. A. Western blot for NR2F1, P-p38, p38, p-ERK, total ERK, SOX9, RARβ, p27 and GAPDH from shControl and shMDK SK-Mel-147 cells. The ratio of p-p38 to p-ERK was calculated by densitometry. **B.** Western blot for NR2F1 in the nuclear fraction and total p38 in the cytosolic fraction from shMDK SK-Mel-147 cells transfected with siC/sip38 (75nM, 48h). Lamin B1 and GAPDH are loading control proteins. **C.** SK-Mel-147 cells were seeded in 2D and then treated with SB203580 (dose curve, left panel) and with 5 μM and 0.5 μM TAK715 (right panel) for 24 hours in serum-free media. Western blots for the indicated targets are shown. MK2 (phosphorylated and total) levels were measured as a p38 target. **D.** SOX9, RAB, and SOX9 mRNA levels were measured by qRT-PCR from shControl and shMDK SK-Mel-147 cells. Unpaired t-test**. E.** SK-Mel-147 cells were seeded in 2D and then treated with Alectinib for 24 hours. qRT-PCR and western blots for the indicated targets are shown. Nuclear extraction was used to detect NR2F1. The ratio of p-p38 to p-ERK was calculated. Unpaired t-test**. F.** SK-Mel-147 cells were seeded in 2D and then transfected with siControl and siALK for 48 hours. qPCR and western blots for the indicated targets are shown. Nuclear extraction was used to detect NR2F1. Numbers represent densitometry analysis for the NR2F1 band over Histone 3. Unpaired t-test**.**

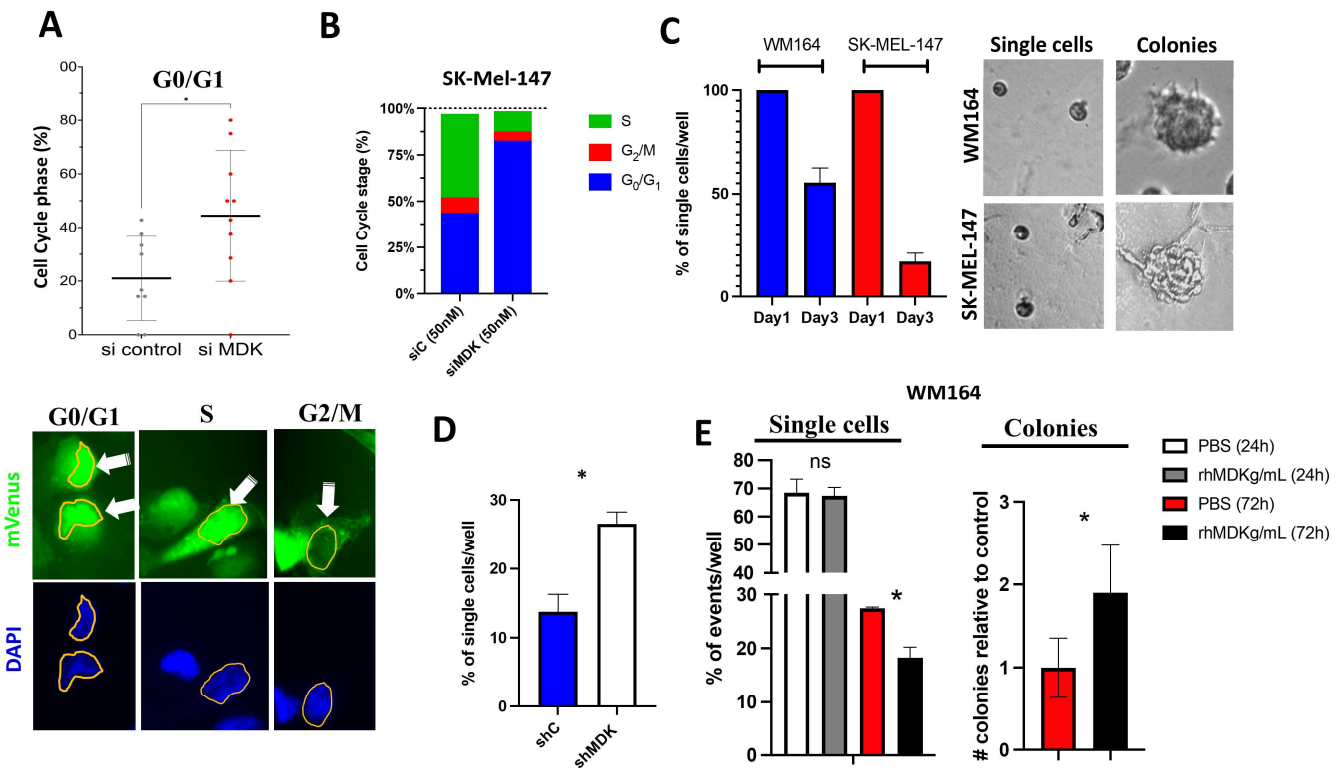

Figure 3. A. SK-Mel-147 cells stably expressing mVenus reporter were transfected with siControl or siMDK and after 48 hours cells were fixed and the percentage of cells in G0/G1 phases was plotted. Representative images for the indicated cell cycle phases are shown. Unpaired t-test. **B.** SK-Mel-147 cells were transfected with siMDK or siControl. Forty-eight hours later cell cycle analysis was done by FACS. **C.** SK-Mel-147 and WM164 cells were seeded on 3D Matrigel. Number of single cells per wells at day 1 and 3 was counted. Representative images for single cells and colonies are shown. **D.** Percentage of single cells on day 3 in shControl vs. shMDK SK-Mel-147 cell lines. Mann-Whitney. **E.** WM164 cells were seeded in 3D and percentages of single cells were measured 24h in PBS (white bars) and rhMDK (grey bars, 20 ng/ml). Three days after treatment the number of single cells and colonies were measured in PBS (red bars) vs. MDK (black bars, 20 ng/ml, daily). Number of single cell events were counted (3 wells/condition, number of events counted=50-100). Representative of two experiments. Unpaired t-test.

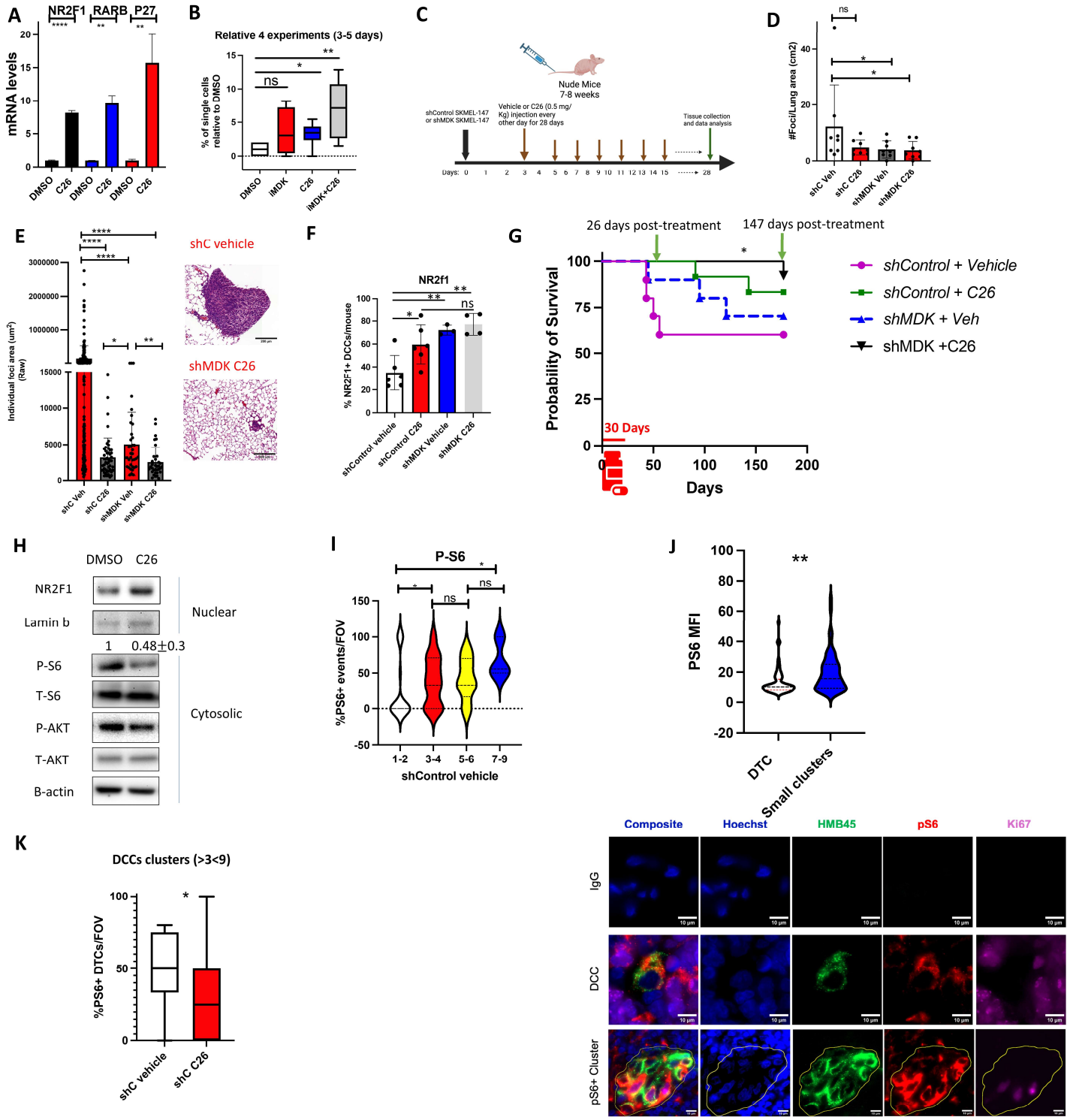

Figure 4. A. SK-Mel-147 cells were treated with C26 (1.0 μM) for 48h. Relative mRNA levels of NR2F1, RARβ and p27 was plotted. Unpaired t-test. **B**. SK-Mel-147 cells were seeded in Matrigel and treated with vehicle, compound 26 and MDK inhibitor. Quantification of single cells at 5 days after respective treatment groups. N= 4 experiments. Mann-Whitney test. **C.** Schematic model for the i.v. injection of shControl and shMDK SK-Mel-147 cells (100,000 cells/mouse) into nude mice followed by treatment with vehicle or C26 for one month. **D&E.**

Collected lung as shown in **C** were stained by H&E and number (**D**) and size (**E**) of metastasis were measured. Representative images of macrometastasis and micrometastasis are shown. Scale bar= 200 um. **F.** Percentage of lung NR2F1+ DCCs in each condition. N= ~200 DCCs/group, 4-6 animals/group. **G.** Same schematic model as in **C** was followed and mice were euthanized when morbidity signs were observed. N=8 mice/group. Gehan-Breslow-Wilcoxon test. **H.** SK-Mel-147 cells were treated with C26 for 24 h and nuclear and cytosolic fractions were collected and plotted against the indicated antigens. **I.** Collected lung from shControl +vehicle group as shown in **Fig. 4C** were stained by IF for vimentin and p-S6. The percentage of DCC positive for PS6 is shown in each group. N= 6 mice. **J.** PS6 signal in solitary DCCs vs. DCC clusters (3-9 cells) from LN+ biopsies was plotted. N= 6 patients. Representative pictures of solitary DCC and clusters of DCCs. **K**. DCC cluster with more than 3 DCC and less than 9 DCCs per field of view (FOV) were stained for PS6 and the percentage of positive cells was plotted for the indicated groups. N= 6 mice/group.

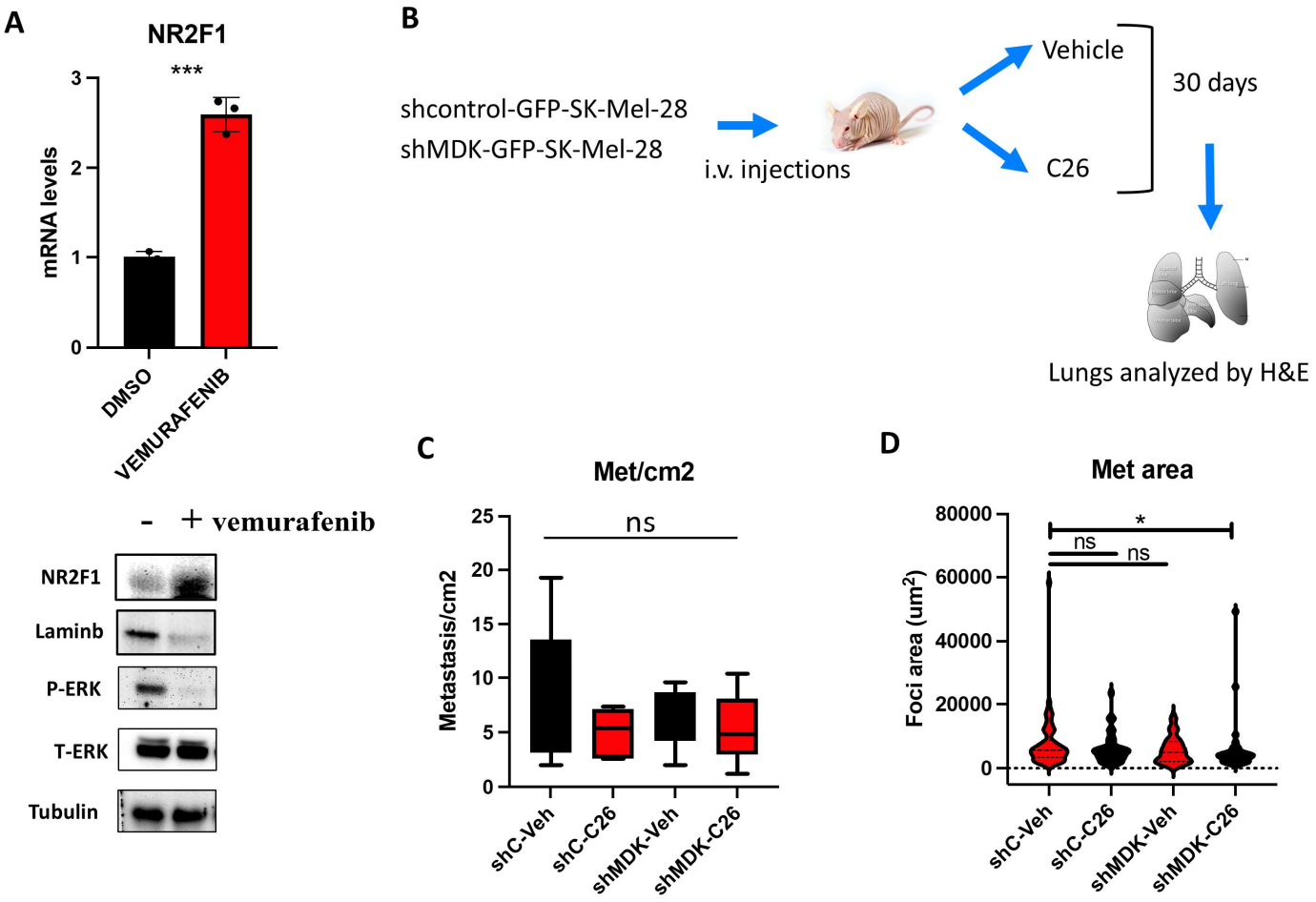

Figure 5. A. NR2F1 mRNA and protein levels in SK-Mel-28 cells treated with vehicle or vemurafenib for 24 h. Unpaired t-test. **B.** Schematic model for the i.v. injection of shControl and shMDK SK-Mel-28 cells (one million cells/mouse) into nude mice followed by treatment with vehicle or C26 for one month. **C&D.** Collected lung as shown in **B** were stained by H&E and number (**C**) and size (**D**) of metastasis were measured. N=5 mice/group. Mann Whitney.

References

1 Ulmer, A. *et al.* Quantitative measurement of melanoma spread in sentinel lymph nodes and survival. *PLoS Med* **11**, e1001604, doi:10.1371/journal.pmed.1001604 (2014).

2 Werner-Klein, M. *et al.* Genetic alterations driving metastatic colony formation are acquired outside of the primary tumour in melanoma. *Nature communications* **9**, 595, doi:10.1038/s41467-017-02674-y (2018).

3 Ulmer, A. *et al.* Detection of melanoma cells displaying multiple genomic changes in histopathologically negative sentinel lymph nodes. *Clinical cancer research : an official journal of the American Association for Cancer Research* **11**, 5425-5432, doi:10.1158/1078-0432.CCR-04-1995 (2005).

4 Cerezo-Wallis, D. *et al.* Midkine rewires the melanoma microenvironment toward a tolerogenic and immune-resistant state. *Nature medicine* **26**, 1865-1877, doi:10.1038/s41591-020-1073-3 (2020).

5 Olmeda, D. *et al.* Whole-body imaging of lymphovascular niches identifies pre-metastatic roles of midkine. *Nature* **546**, 676-680, doi:10.1038/nature22977 (2017).

6 Sosa, M. S. *et al.* NR2F1 controls tumour cell dormancy via SOX9- and RARbeta-driven quiescence programmes. *Nature communications* **6**, 6170, doi:10.1038/ncomms7170 (2015).

7 Khalil, B. D. *et al.* An NR2F1-specific agonist suppresses metastasis by inducing cancer cell dormancy. *The Journal of experimental medicine* **219**, doi:10.1084/jem.20210836 (2022).

8 Borriello, L. *et al.* Primary tumor associated macrophages activate programs of invasion and dormancy in disseminating tumor cells. *Nature communications* **13**, 626, doi:10.1038/s41467-022-28076-3 (2022).

9 Chery, L. *et al.* Characterization of single disseminated prostate cancer cells reveals tumor cell heterogeneity and identifies dormancy associated pathways. *Oncotarget* **5**, 9939-9951 (2014).

10 Borgen, E. *et al.* NR2F1 stratifies dormant disseminated tumor cells in breast cancer patients. *Breast cancer research : BCR* **20**, 120, doi:10.1186/s13058-018-1049-0 (2018).

11 Aguirre-Ghiso, J. A., Liu, D., Mignatti, A., Kovalski, K. & Ossowski, L. Urokinase receptor and fibronectin regulate the ERK(MAPK) to p38(MAPK) activity ratios that determine carcinoma cell proliferation or dormancy in vivo. *Mol Biol Cell* **12**, 863-879 (2001).

12 Kodama, T. *et al.* Antitumor activity of the selective ALK inhibitor alectinib in models of intracranial metastases. *Cancer Chemother Pharmacol* **74**, 1023-1028, doi:10.1007/s00280-014-2578-6 (2014).

13 Peters, S. *et al.* Alectinib versus Crizotinib in Untreated ALK-Positive Non-Small-Cell Lung Cancer. *N Engl J Med* **377**, 829-838, doi:10.1056/NEJMoa1704795 (2017).

14 Ross-Munro, E. *et al.* Midkine: The Who, What, Where, and When of a Promising Neurotrophic Therapy for Perinatal Brain Injury. *Front Neurol* **11**, 568814, doi:10.3389/fneur.2020.568814 (2020).

15 Spencer, S. L. *et al.* The proliferation-quiescence decision is controlled by a bifurcation in CDK2 activity at mitotic exit. *Cell* **155**, 369-383, doi:10.1016/j.cell.2013.08.062 (2013).

16 Chapman, P. B. *et al.* Improved survival with vemurafenib in melanoma with BRAF V600E mutation. *N Engl J Med* **364**, 2507-2516, doi:10.1056/NEJMoa1103782 (2011).

17 Davies, H. *et al.* Mutations of the BRAF gene in human cancer. *Nature* **417**, 949-954, doi:10.1038/nature00766 (2002).

18 Dai, L. C. *et al.* In vitro and in vivo suppression of hepatocellular carcinoma growth by midkine-antisense oligonucleotide-loaded nanoparticles. *World J Gastroenterol* **15**, 1966-1972, doi:10.3748/wjg.15.1966 (2009).

19 Fluegen, G. *et al.* Phenotypic heterogeneity of disseminated tumour cells is preset by primary tumour hypoxic microenvironments. *Nature cell biology* **19**, 120-132, doi:10.1038/ncb3465 (2017).

20 Ossowski, L. & Reich, E. Changes in malignant phenotype of a human carcinoma conditioned by growth environment. *Cell* **33**, 323-333, doi:10.1016/0092-8674(83)90414-2 (1983).

21 Aguirre Ghiso, J. A., Kovalski, K. & Ossowski, L. Tumor dormancy induced by downregulation of urokinase receptor in human carcinoma involves integrin and MAPK signaling. *J Cell Biol* **147**, 89-104, doi:10.1083/jcb.147.1.89 (1999).

22 Akturk, G., Sweeney, R., Remark, R., Merad, M. & Gnjatic, S. Multiplexed Immunohistochemical Consecutive Staining on Single Slide (MICSSS): Multiplexed Chromogenic IHC Assay for High-Dimensional Tissue Analysis. *Methods Mol Biol* **2055**, 497-519, doi:10.1007/978-1-4939-9773-2_23 (2020).